



**HAL**  
open science

## Properties of $\gamma$ -decaying isomers in the $^{100}\text{Sn}$ region populated in fragmentation of a $^{124}\text{Xe}$ beam

G. Häfner, K. Moschner, A. Blazhev, P. Boutachkov, P.J. Davies, R. Wadsworth, F. Ameil, H. Baba, T. Bäck, M. Dewald, et al.

### ► To cite this version:

G. Häfner, K. Moschner, A. Blazhev, P. Boutachkov, P.J. Davies, et al.. Properties of  $\gamma$ -decaying isomers in the  $^{100}\text{Sn}$  region populated in fragmentation of a  $^{124}\text{Xe}$  beam. Phys.Rev.C, 2019, 100 (2), pp.024302. 10.1103/PhysRevC.100.024302 . hal-02266317

**HAL Id: hal-02266317**

**<https://hal.science/hal-02266317>**

Submitted on 15 Dec 2020

**HAL** is a multi-disciplinary open access archive for the deposit and dissemination of scientific research documents, whether they are published or not. The documents may come from teaching and research institutions in France or abroad, or from public or private research centers.

L'archive ouverte pluridisciplinaire **HAL**, est destinée au dépôt et à la diffusion de documents scientifiques de niveau recherche, publiés ou non, émanant des établissements d'enseignement et de recherche français ou étrangers, des laboratoires publics ou privés.

# Properties of $\gamma$ -decaying isomers in the $^{100}\text{Sn}$ region populated in fragmentation of a $^{124}\text{Xe}$ beam

G. Häfner,<sup>1,2,a</sup> K. Moschner,<sup>1</sup> A. Blazhev,<sup>1</sup> P. Boutachkov,<sup>3</sup> P. J. Davies,<sup>4</sup> R. Wadsworth,<sup>4</sup> F. Ameil,<sup>3</sup> H. Baba,<sup>5</sup> T. Bäck,<sup>6</sup> M. Dewald,<sup>1</sup> P. Doornenbal,<sup>5</sup> T. Faestermann,<sup>7</sup> A. Gengelbach,<sup>8</sup> J. Gerl,<sup>3</sup> R. Gernhäuser,<sup>7</sup> S. Go,<sup>9</sup> M. Górska,<sup>3</sup> H. Grawe,<sup>3</sup> E. Gregor,<sup>10</sup> H. Hotaka,<sup>11</sup> T. Isobe,<sup>5</sup> D. G. Jenkins,<sup>4</sup> J. Jolie,<sup>1</sup> H. S. Jung,<sup>12</sup> I. Kojouharov,<sup>3</sup> N. Kurz,<sup>3</sup> M. Lewitowicz,<sup>13</sup> G. Lorusso,<sup>5</sup> R. Lozeva,<sup>2</sup> E. Merchan,<sup>10</sup> F. Naqvi,<sup>14</sup> H. Nishibata,<sup>15</sup> D. Nishimura,<sup>16</sup> S. Nishimura,<sup>5</sup> N. Pietralla,<sup>10</sup> H. Schaffner,<sup>3</sup> P.-A. Söderström,<sup>5</sup> K. Steiger,<sup>7</sup> T. Sumikama,<sup>17</sup> J. Taprogge,<sup>18,19</sup> P. Thöle,<sup>1</sup> H. Watanabe,<sup>20</sup> N. Warr,<sup>1</sup> V. Werner,<sup>10,14</sup> Z. Y. Xu,<sup>9</sup> A. Yagi,<sup>15</sup> K. Yoshinaga,<sup>11</sup> and Y. Zhu<sup>11</sup>

<sup>1</sup>*Institut für Kernphysik, Universität zu Köln, D-50937 Köln, Germany*

<sup>2</sup>*CSNSM, CNRS/IN2P3, Université Paris-Saclay, F-91405 Orsay-Campus, France*

<sup>3</sup>*GSI Helmholtzzentrum für Schwerionenforschung GmbH, D-62491 Darmstadt, Germany*

<sup>4</sup>*Department for Physics, University of York, York, YO10 5DD, UK*

<sup>5</sup>*RIKEN Nishina Center, Wako-shi, 351-0198 Saitama, Japan*

<sup>6</sup>*Department of Physics, KTH Stockholm, SE-100 44 Stockholm, Sweden*

<sup>7</sup>*Physics Department, Technische Universität München, D-80333 München, Germany*

<sup>8</sup>*Department of Physics and Astronomy, Uppsala University, SE-75120 Uppsala, Sweden*

<sup>9</sup>*Department of Physics, University of Tokyo, Tokyo 113-8654, Japan*

<sup>10</sup>*Institut für Kernphysik, Technische Universität Darmstadt, D-64289, Germany*

<sup>11</sup>*Department of Physics, Tokyo University of Science, Chiba 278-8510, Japan*

<sup>12</sup>*Department of Physics, Chung-Ang University, Seoul 156-756, Republic of Korea*

<sup>13</sup>*Grand Accélérateur National d'Ions Lourds (GANIL),*

*CEA/DSM-CNRS/IN2P3, F-14076 Caen Cedex, France*

<sup>14</sup>*Department of Physics and Wright Nuclear Structure Laboratory, Yale University, New Haven, CT 06520, USA*

<sup>15</sup>*Department of Physics, Osaka University, Osaka 560-0043, Japan*

<sup>16</sup>*Department of Physics, Tokyo City University, Tokyo 158-8557, Japan*

<sup>17</sup>*Department of Physics, Faculty of Science, Tohoku University, Sendai 980-8578, Japan*

<sup>18</sup>*Institute of the Structure of Matter, CSIC Madrid, ES-28006 Madrid, Spain*

<sup>19</sup>*Universidad Autónoma de Madrid, ES-28049 Madrid, Spain*

<sup>20</sup>*Department of Physics, Beihang University, Beijing 100083, China*

(Dated: July 5, 2019)

A systematic study of microsecond  $\gamma$ -decaying isomers around  $^{100}\text{Sn}$  produced in a fragmentation reaction of a  $^{124}\text{Xe}$  beam at 345 MeV/u at the Radioactive Ion Beam Factory of the RIKEN Nishina Center in Saitama, Japan was performed. Half-lives of isomeric states in that region were remeasured allowing to improve the currently available experimental information. Reduced transition probabilities were deduced and compared to shell-model calculations in various model spaces. The recently reported low-energy transitions in  $^{92}\text{Rh}$  and  $^{96}\text{Ag}$  were remeasured with improved precision. Additionally, experimental information on isomeric ratios, among which five new ones, were extracted and compared to a previous experimental study and the sharp cut-off model of fragmentation reaction.

PACS numbers: 23.20.Lv, 27.60.+j, 23.35.+g, 21.10.Tg, 21.60.Cs, 25.70.Mn

## I. INTRODUCTION

The  $N = Z (= 50)$  nucleus  $^{100}\text{Sn}$  is the heaviest self-conjugate doubly-magic nucleus and lies close to the proton drip line. The region of  $N \sim Z$  nuclei around  $^{100}\text{Sn}$  exhibits many nuclear structure phenomena and is important for the astrophysical rapid proton capture process [1, 2]. An extensive review on experimental and theoretical work in that region can be found in Ref. [3] and references therein. Some highlights include the super-allowed Gamow-Teller transition in  $\beta^+/\text{EC}$  decay due to the fully filled proton  $\pi(0g_{9/2})$  and empty neutron  $\nu(0g_{7/2})$  orbitals in  $^{100}\text{Sn}$  [4] or the influence of the pn-interaction manifesting itself in a strong  $T = 0$  ( $g_{7/2}^2$ )<sub>9</sub><sup>+</sup> binding [5].

A large number of isomeric states for nuclei ‘south-west’ of  $^{100}\text{Sn}$  result from shell effects below  $N, Z = 50$ . For example, the influence of the  $\pi\nu(0g_{9/2})$  orbitals gives rise to high-spin isomers and  $8^+$  seniority isomers in the  $N = 50$  isotones [6–8]. Core-excitations across the  $N = 50$  closed shell are manifested in excited states of nuclei close to  $^{100}\text{Sn}$  which can be identified by the existence of excited states beyond the restricted model space. In fusion-evaporation studies, core-excited states in  $^{96}\text{Pd}$  [9, 10],  $^{97}\text{Ag}$  [11] and  $^{99}\text{Cd}$  [12] were observed. Recently, isomers involving an excitation across the  $N = 50$  shell closure were found in  $^{96}\text{Ag}$  [13] and  $^{98}\text{Cd}$  [14, 15]. The de-excitation of all these isomeric states can be studied through  $\gamma$ -ray spectroscopy at in-flight separation facilities if the half-lives  $T_{1/2}$  are sufficiently long to survive the flight path (in the order of  $\mu\text{s}$ ). Furthermore, the half-lives of excited states are used to calculate reduced transition probabilities  $B(\sigma\lambda)$  for a given multipolarity  $\sigma\lambda$ , which can then be compared with theoretical models.

<sup>a</sup> Corresponding author: ghaefner@ikp.uni-koeln.de

Around  $^{100}\text{Sn}$ , the nuclear shell-model is most often the theory of choice, and, depending on the isotope of interest, different model spaces and effective interactions are used (see for example Tab. 3 of Ref. [3]). For  $A \sim 90$  nuclei ‘south-west’ of  $^{100}\text{Sn}$ , the PG  $\pi\nu$  ( $1p_{1/2} 0g_{9/2}$ ) model space provides a good description of excitation energies and transition strengths, see for example Refs. [16, 17]. Large-scale shell model calculations (LSSM) in the GDS  $\pi\nu$  ( $0g, 1d, 2s$ ) model space predict a core-excited  $6^+$  isomer in  $^{100}\text{Sn}$  with a half-life ranging from a few 100 ns to 2.6  $\mu\text{s}$  and a transition energy below 260 keV [3, 18].

Recently, Park *et al.* [19] published an article on properties of  $\gamma$ -decaying isomers around  $^{100}\text{Sn}$  and isomeric ratios. Highlights of this study include the discovery of two new low-energy isomeric transitions in  $^{92}\text{Rh}$  and  $^{96}\text{Ag}$  and new constraints on  $T_{1/2}$  and  $E_\gamma$  of the predicted isomer in  $^{100}\text{Sn}$ . The results from the present work were obtained in a similar experiment employing the same reaction, thus, providing complementary information on isomers in that region.

This paper is organised as follows: the experimental setup and data analysis are described in Sec. II. Results from this analysis are presented and discussed in Sec. III. The latter section also includes a comparison with different model calculations. Finally, Sec. IV provides a summary of this work.

## II. EXPERIMENTAL PROCEDURE AND DATA ANALYSIS

Neutron-deficient nuclei around  $^{100}\text{Sn}$  were produced in a fragmentation reaction of a 345 MeV/u  $^{124}\text{Xe}$  beam on a 4 mm thick  $^9\text{Be}$  target at the Radioactive Ion Beam Factory (RIBF) of the RIKEN Nishina Center. The experiment was part of the EURICA campaign [20] and, previously, results from this experiment have been published in Refs. [21–24]. A secondary cocktail beam was in-flight separated in the first stage of the fragment separator BigRIPS. Further separation and an event-by-event particle identification were provided in the second stage of BigRIPS using the  $B\rho$ -TOF- $\Delta E$ -method [25, 26]. Figure 1 shows an identification plot of atomic charge number  $Z$  against mass-to-charge ratio  $A/Q$  in the range of  $40 \leq Z \leq 50$  illustrating the clean particle separation of this setup. The majority of secondary ions are fully stripped so that  $Q = Z$ .

Secondary ions were implanted in a modified version of the active stopper SIMBA [4, 27] located at focal point F11 of the ZeroDegree spectrometer [26]. The flight time for different ions from the target position up to F11 was calculated with LISE++ [28] and was around 740 ns in the lab frame. The active stopper was surrounded by the Euroball RIKEN Cluster Array (EURICA), which contained 84 HPGe detectors for high-resolution and high-efficiency  $\gamma$ -ray spectroscopy. During the experiment, 81 channels of EURICA were active. Long-lived isomeric decays were detected using digital  $\gamma$ -finder (DGF) modules with an acquisition range of up to 90  $\mu\text{s}$ . Internal conversion (IC) electrons as well as particles from other decay modes ( $\beta$ ,  $\beta p$ ,  $p$ ) were measured in the silicon detectors of the active stopper if the energy was above 150 keV and the half-life greater than the 400  $\mu\text{s}$  average dead time of SIMBA after implantation.

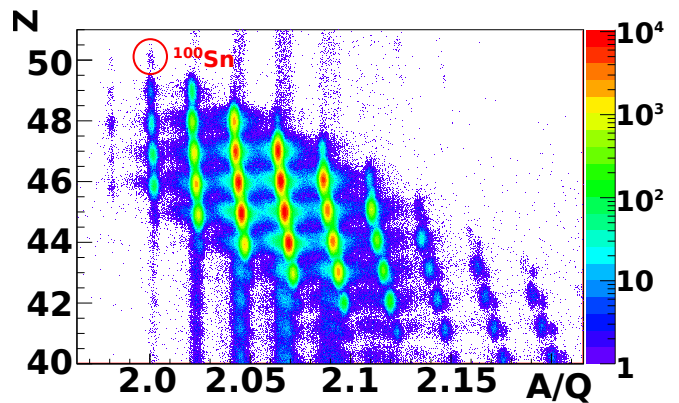


Figure 1. (Colour online) Particle identification plot of secondary ions produced in this experiment and implanted in the active stopper detector at the end of the ZeroDegree spectrometer (see text for details). Events from the identification of  $^{100}\text{Sn}$  isotopes are highlighted as a reference.

Ion selection cuts in the particle identification plot with low contamination (less than 0.5% in most cases) were applied in order to study characteristic  $\gamma$ -rays following the decay of an isomeric state. The half-lives were measured with a start time given by a plastic scintillator located at F11 and the stop signal time from the EURICA acquisition branch. An energy gate on  $\gamma$ -rays belonging to the decay cascades of an isomeric state was utilised to generate time spectra. Half-lives were extracted by simultaneously fitting the background (either constant or time-dependent) and non-subtracted time spectra gated on transitions below the isomer using the maximum likelihood method. Since the choice of fit region influences the resulting half-lives, we have applied the following steps to determine appropriate fit regions for the different cases. First, a numerical derivative of the logarithmic time spectrum was constructed. Second, the fit range was systematically varied and the systematic uncertainty due to the fit range was extracted from the  $1\sigma$  range. The half-life measurement was limited to  $T_{1/2}$ -values up to around 100  $\mu\text{s}$  with the lower limit determined by the flight time. These results were used to estimate new  $B(\sigma\lambda)$  values using known branching ratios (BR) and IC coefficients  $\alpha$ . The IC coefficients were calculated with the program BRICC [29].

Experimental isomeric ratios  $R_{exp}$  were obtained using Eq. 5 from Ref. [30] modified by a correction term for prompt flash events  $f_1$ , resulting in

$$R_{exp} = \frac{Y}{N_{imp} f_1 f_2 f_3}. \quad (1)$$

$Y$  is the number of isomer decays extracted from the measured depopulating  $\gamma$ -ray intensity (corrected for detection efficiency and internal conversion).  $N_{imp}$  the number of implanted ions and  $f_{1-3}$  are factors correcting for prompt flash events, in-flight decay and the finite detection window, respectively. The use of  $f_1$  has been adopted from Refs. [31, 32]:

$$f_1 = 1 - \frac{N_p}{N_{imp} N_C}, \quad (2)$$

where  $N_p$  is the number of prompt flash events around time  $t = 0$  and  $N_C = 81$  the number of active detectors.  $f_2$  takes into account isomeric decays during the flight time from the production target to the implantation zone and is given by (adapted from Eq. 6 in Ref. [30]):

$$f_2 = \exp \left[ -\lambda^0 \left( \sum_i \frac{\text{TOF}_i}{\gamma_i} \right) \right], \quad (3)$$

with  $\lambda^0$  being the decay constant for fully stripped ions summed over all decay branches,  $\text{TOF}_i$  the time of flight for the  $i$ -th segment through the separator and  $\gamma_i$  the relativistic constant for that respective segment.  $f_3$  corrects for the finite detection window provided by the acquisition system and reads (see Eq. 8 of Ref. [30]):

$$f_3 = e^{-\lambda t_i} - e^{-\lambda t_f}. \quad (4)$$

$t_i$  and  $t_f$  are initial and final time of the experimental detection window and are 0  $\mu\text{s}$  and 90  $\mu\text{s}$  if no further time constraints are applied.  $f_1$  is generally close to unity (0.90 to 0.98) while  $f_2$  yields the dominating correction for short-lived isomers and  $f_3$  for long-lived isomers.

If two isomers decay successively and the lower one is fed by the upper isomer, one has to correct the lower isomeric ratio for the feeding from the higher-lying isomer. If we denote the upper isomeric ratio calculated by Eq. 1 as  $R_U$  and the branching from the upper to the lower isomer as  $b_{UL}$ , the corrected lower isomeric ratio  $R_L^{cor}$  can be calculated (taken from Eq. 6 in Ref. [33] and modified for the  $f_1$  correction term):

$$\begin{aligned} R_L^{cor} &= \frac{Y_L}{N_{imp} f_1 f_2^L f_3^L} - b_{UL} \frac{R_U}{f_1 f_2^L f_3^L} \\ &\times \left[ f_2^U \frac{\lambda_U (f_3^U - f_3^L)}{\lambda_L - \lambda_U} \right. \\ &\left. + \frac{\lambda_U^0}{\lambda_L^0 - \lambda_U^0} f_3^L (f_2^U - f_2^L) \right], \end{aligned} \quad (5)$$

Where the indices  $U$  and  $L$  denote the upper (U) and lower (L) isomeric state. In this work, such a correction was applied to the ( $14^+$ ) isomer in  $^{94}\text{Pd}$ , the ( $15^+$ ) state in  $^{96}\text{Ag}$ , the ( $23/2^+$ ) isomer in  $^{95}\text{Ag}$  and the ( $8^+$ ) isomer in  $^{98}\text{Cd}$ .

### III. RESULTS AND DISCUSSION

#### A. Half-lives and Transition Strengths of Isomeric States

Half-lives of 17 isomeric states in neutron-deficient nuclei below  $^{100}\text{Sn}$  have been remeasured. Figure 2 shows the time spectra and the obtained  $T_{1/2}$  values for each state. The new half-lives are consistent with literature values and, in some cases, reduce the relative uncertainty. Most of the time, gates on multiple transitions belonging to the cascade below an isomer have been used to generate time spectra. For the 4207 keV ( $12^+$ )  $\rightarrow$  ( $8^+$ ) transition in  $^{98}\text{Cd}$  also the single- and double-escape peaks were taken into account. Note that for high

statistics cases the time dependence of the background originates mainly from Compton scattered  $\gamma$ -rays of the isomers and has therefore has little influence on the obtained  $T_{1/2}$  value.

From these experimental results, reduced transition probabilities are deduced for a comparison with theoretical models. Shell-model (SM) calculations in the PG model space have been performed with the code NUSHELLX [34] employing the effective, isospin-symmetric SLGT0PN interaction [35] provided in the NUSHELLX package. Excitation energies and transition strengths were calculated. Standard effective charges of (a)  $e_\pi = 1.5e$ ,  $e_\nu = 0.5e$  and values of (b)  $e_\pi = 1.72e$ ,  $e_\nu = 1.44e$  tuned to proton-rich  $A \sim 90$  nuclei [36] were chosen to obtain theoretical  $B(\sigma\lambda)$  values. For  $^{98}\text{Ag}$  having  $N = 51$ , calculations were performed including the proton  $\pi$  ( $1p_{1/2}$ ,  $0g_{9/2}$ ) and neutron  $\nu$  ( $0g_{7/2}$ ,  $1d_{5/2}$ ,  $0h_{11/2}$ ) orbitals using the SR88MHJM interaction [3, 37]. The respective effective charges were chosen to be (a)  $e_\pi = 1.5e$ ,  $e_\nu = 0.5e$  and (b)  $e_\pi = 1.72e$ ,  $e_\nu = 1.5e$ . The latter neutron effective charge was modified to reproduce the experimental  $B(E2: 4^+ \rightarrow 6^+)$  strength in  $^{98}\text{Ag}$ . A comparison of theoretical and experimental transition probabilities is presented in Tab. I.

In general, the experimental  $B(\sigma\lambda)$  values are well reproduced by the SM calculation when adapting the effective charges to  $A \sim 90$  nuclei. Figure 3 shows a graphical comparison between experimental and theoretical results to visualise this fact. Large deviations are only present in the ( $8^+$ ) isomers in  $^{92,94}\text{Ru}$  and the core-excited ( $12^+$ ) isomer in  $^{98}\text{Cd}$ . The anomalous behaviour of the  $B(E2: 8^+ \rightarrow 6^+)$  strength in  $^{94}\text{Ru}$  can be explained by the breakdown of the seniority scheme in the  $N = 50$  isotones, due to a premature filling of the  $0g_{9/2}$  orbital, caused by scattering of neutrons from the  $1p_{1/2}$  orbital [9, 40]. For an extensive discussion on the core-excited ( $12^+$ ) isomer in  $^{98}\text{Cd}$  the reader is referred to Refs. [3, 14, 15].

#### B. Low-energy Isomeric Transitions

In the studied nuclei ( $40 \leq Z \leq 50$ ), low-energy  $E2$  transitions of less than 100 keV are dominated by an internal conversion branch over the emission of a  $\gamma$ -ray. As the conversion coefficient dramatically increases with decreasing transition energy, its exact knowledge is very important for a proper calculation of experimental  $B(E2)$  strengths. Low-energy HPGe spectra could be contaminated by x-rays or affected by electronic threshold effects, thus making re-measurement and confirmation of reported low-energy transitions highly desirable. Two new low-energy isomeric transitions in  $^{92}\text{Rh}$  and  $^{96}\text{Ag}$  were first reported in Ref. [19]. Our work is an independent measurement and preliminary results were presented recently in Ref. [41]. In this section the final results confirming the low-energy isomeric transitions and further results improving the experimental information are presented.

In general, the low-energy region of the  $\gamma$ -ray spectrum is dominated by prompt flash events. By limiting the DGF time window in the offline analysis, these events are suppressed and low-energy  $\gamma$ -rays belonging to isomeric decays are exposed. The time range has to be chosen according to the half-life of the isomer.

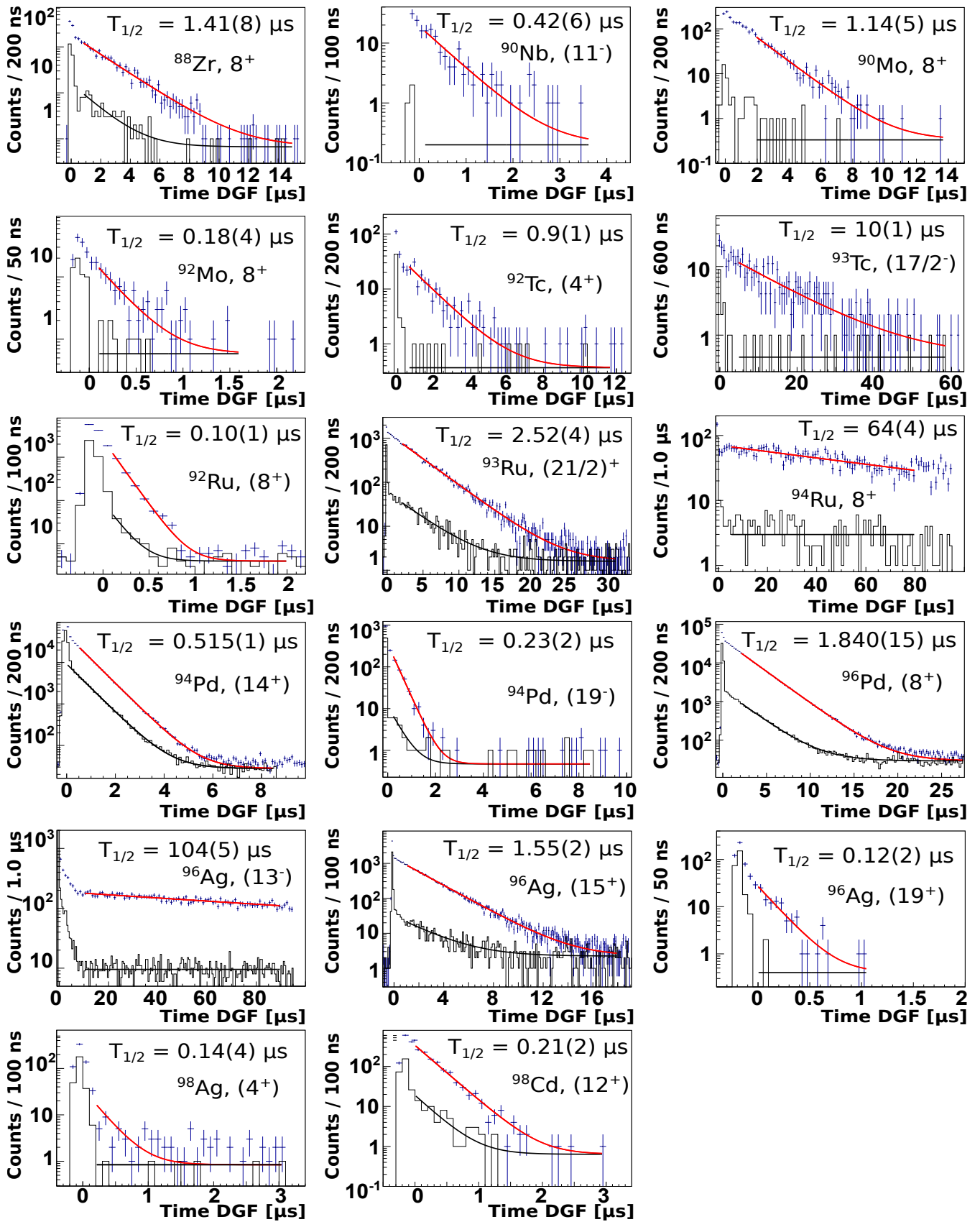


Figure 2. (Colour online) Time spectra and decay curves used to obtain the half-lives of  $\gamma$ -decaying isomers. The decay curves are fitted using a single exponential function (red) together with a constant or time-dependent background term (black). The on-peak gated time distributions are plotted in blue and the respective background counts are given as histograms in black. Each figure is labelled with the isotope, isomeric spin, parity and its respective half-life.

Table I. Electric transition strengths experimentally deduced and calculated in this work. Unless denoted otherwise, the calculations are performed with the SLGT0PN interaction in the PG model space. Two different sets of effective charges (a)  $e_\pi=1.5 e$ ,  $e_\nu = 0.5 e$  and (b)  $e_\pi = 1.72 e$ ,  $e_\nu = 1.44 e$  were used if not indicated otherwise. Energies given with an uncertainty are experimentally deduced in this work and will be discussed in Sec. III B. Spin and parity assignments are taken from the literature [42]. Branching ratios are taken from Ref. [38] for the  $(17/2^-)$  state in  $^{93}\text{Tc}$ , deduced from intensities given in Ref. [13] for the  $(13^-)$  state in  $^{96}\text{Ag}$  and otherwise taken from Ref. [19], where needed.

Nucleus	$J_i^\pi$	$\sigma\lambda$	$E_\gamma$ [keV]	$J_f^\pi$	$B(\sigma\lambda)$ [W.u.]		
					Exp.	SM (a)	SM (b)
$^{88}\text{Zr}$	$8^+$	$E2$	77	$6^+$	1.65(9)	0.47	2.25
$^{90}\text{Nb}$	$(11^-)$	$E2$	71	$(9^-)$	1.7(5)	1.49	1.47
$^{90}\text{Mo}$	$8^+$	$E2$	63	$6^+$	2.8(2)	1.19	3.39
$^{92}\text{Mo}$	$8^+$	$E2$	148	$6^+$	1.4(3)	1.05	1.38
$^{92}\text{Tc}$	$(4^+)$	$E2$	56	$(6^+)$	4.3(5)	2.40	4.28
$^{93}\text{Tc}$	$(17/2^-)$	$E2$	40	$(13/2^-)$	0.47(5)	0.18	0.23
$^{92}\text{Ru}$	$(8^+)$	$E2$	162	$(6^+)$	1.68(17)	0.31	0.89
$^{93}\text{Ru}$	$(21/2^+)$	$E2$	146	$(17/2^+)$	0.101(5)	0.098	0.099
$^{94}\text{Ru}$	$8^+$	$E2$	146	$6^+$	0.0039(2)	0.063	0.083
$^{92}\text{Rh}$	$(4^+)$	$E2$	55.6(1)	$(2^+)$	16(1)	5.89	15.21
$^{94}\text{Pd}$	$(19^-)$	$E3$	1651	$(16^+)$	0.24(3)	0.10 <sup>a</sup>	0.18 <sup>a</sup>
		$E1$	106	$(18^+)$	$2.2(7)\times 10^{-7}$		
	$(14^+)$	$E2$	95	$(12^+)$	2.05(4)	1.93	5.43
$^{96}\text{Pd}$	$(8^+)$	$E2$	106	$(6^+)$	0.408(8)	0.26	0.34
$^{96}\text{Ag}$	$(19^+)$	$E4$	4265	$(15^+)$	1.1(6)	0.70 <sup>b</sup>	
		$E2$	98	$(17^+)$	6.3(13)	3.57 <sup>b</sup>	
	$(15^+)$	$E2$	44.1(2)	$(13^+)$	2.90(10)	2.99	4.27
	$(13^-)$	$E3$	743	$(10^+)$	0.140(8)	0.058 <sup>c</sup>	0.13 <sup>c</sup>
		$E3^d$	486	$(11^+)$	0.59(7)	0.531 <sup>c</sup>	0.694 <sup>c</sup>
$^{98}\text{Ag}$	$(4^+)$	$E2$	107	$(6^+)$	5.0(14)	1.7 <sup>e</sup>	5.0 <sup>e</sup>
$^{98}\text{Cd}$	$(12^+)$	$E4$	4207	$(8^+)$	3.2(4)	0.77 <sup>f</sup>	
		$E2$	49.2 <sup>g</sup>	$(10^+)$	2.1(4)	0.72 <sup>f</sup>	

<sup>a</sup> Calculation in the  $\pi\nu(0f_{5/2}1p0g_{9/2})$  model space taken from Ref. [39].

<sup>b</sup> Core-excited states calculated in the GDS model space taken from Ref. [13].

<sup>c</sup> Calculation in the  $\pi\nu(0f_{5/2}1p0g_{9/2})$  model space taken from Ref. [13].

<sup>d</sup> Assuming a pure  $E3$  transition.

<sup>e</sup> Calculations using the  $\pi(1p_{1/2}0g_{9/2})$  and  $\nu(0g_{7/2}1d_{2s}0h_{11/2})$  shells (see text for details).

<sup>f</sup> Core-excited states calculated in the GDS model space (Refs. [14, 15]).

<sup>g</sup> Transition energy taken from Ref. [19].

For  $^{92}\text{Rh}$ , a time window of  $400 \text{ ns} \leq T_{DGF} \leq 1200 \text{ ns}$  has been chosen. The corresponding time-delayed  $\gamma$ -ray spectrum can be seen in Fig. 4. From the fit, an energy of 55.6(1) keV was obtained, in agreement with 55.3(3) keV from Ref. [19]. The error combines a statistical component from the Gaussian fit as well as the systematic uncertainty due to the time cut and the energy resolution. The time spectrum gated on this energy can be seen in the inset of Fig. 4. The resulting half-life obtained

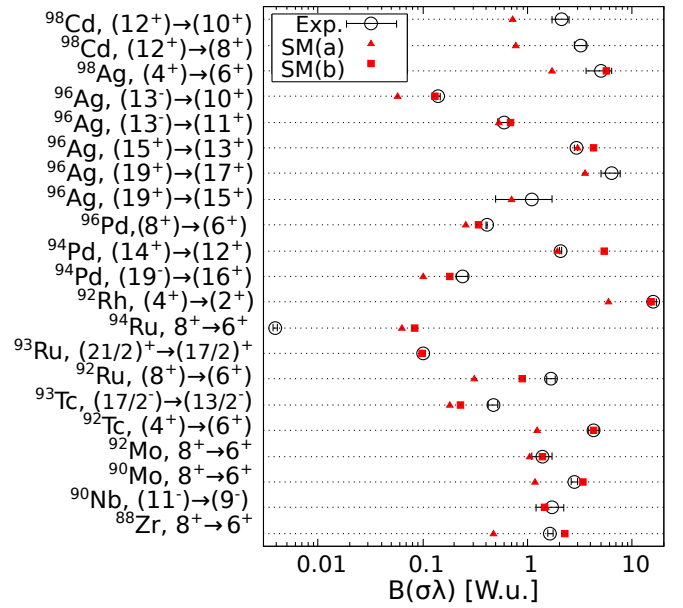


Figure 3. (Colour online) Reduced transition probabilities for isomeric  $\gamma$ -ray transitions. Comparison between experimental and calculated transition strengths. See Tab. I for the description of the labels (a) and (b).

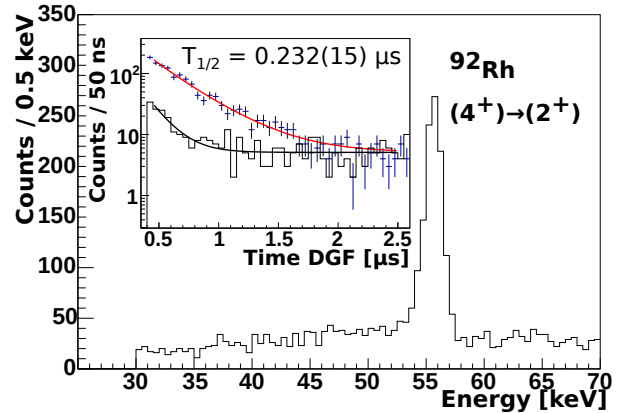


Figure 4. (Colour online) Time-delayed projected  $\gamma$ -ray energy between  $400 \text{ ns} \leq T_{DGF} \leq 1200 \text{ ns}$ . The inset shows the time spectrum and decay curve of the 55 keV transition. Note that this time spectrum was generated by increasing the upper time limit to  $T_{DGF} \leq 3500 \text{ ns}$ .

by fitting an exponential decay curve with a time-dependent background amounts to  $T_{1/2} = 0.232(15) \mu\text{s}$  and is consistent with  $T_{1/2} = 0.23(6) \mu\text{s}$  [19] while improving the uncertainty by a factor of four. This 55 keV transition was proposed to belong to the decay of a new  $(4^+)$  isomer decaying to the  $\beta$ -decaying  $(2^+)$  state in  $^{92}\text{Rh}$ . The reduced transition probability for this case gives a new  $B(E2)$  estimation of 16(1) W.u. This value is consistent with the experimental value from Ref. [19] and is compatible with  $B(E2 : 4^+ \rightarrow 2^+)$ -value from SM calculation in the PG model space using the SLGT0PN (15.2 W.u.) and close to the value from the SLGM [16] (18.3 W.u.) interaction.

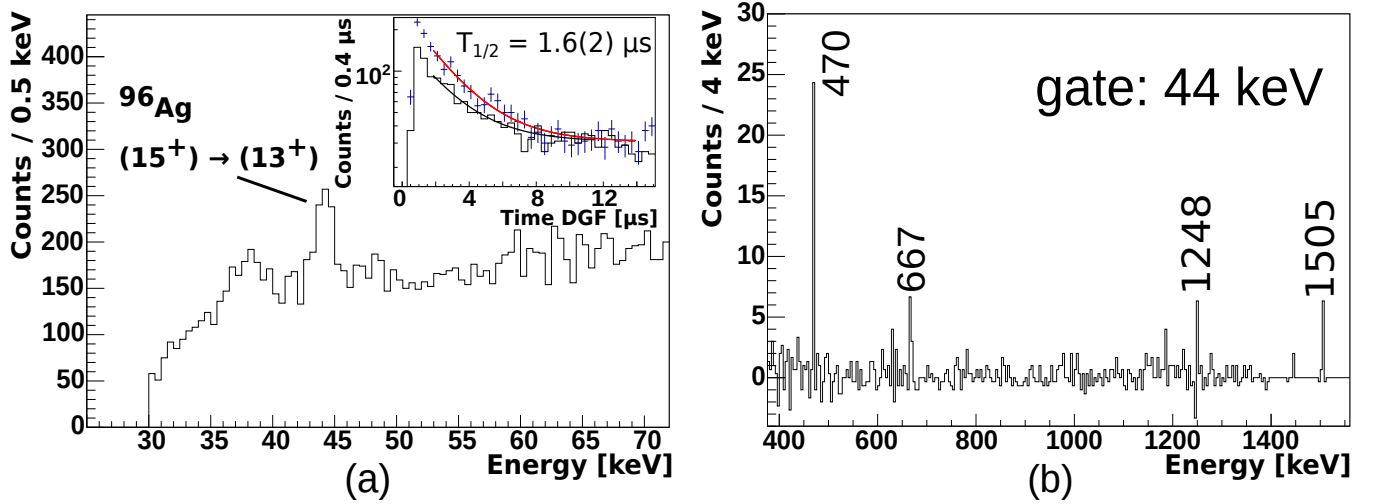


Figure 5. (Colour online) (a) Partial  $\gamma$ -ray spectrum of  $^{96}\text{Ag}$  showing time-delayed  $\gamma$ -ray energies between 800 ns and 3400 ns. The inset shows the time distribution of the 44 keV transition in  $^{96}\text{Ag}$  obtained with a time window of  $800 \text{ ns} \leq T_{DGF} \leq 20 \mu\text{s}$ . (b) Projection of the  $\gamma$ - $\gamma$ -matrix gated on 44 keV. The labelled peaks belong to transitions in  $^{96}\text{Ag}$  following the decay of the  $(15^+)$  isomer.

In the case of the  $1.5 \mu\text{s}$ -isomer in  $^{96}\text{Ag}$ , a time window ranging from 800 ns to 3400 ns was applied. The resulting time-delayed  $\gamma$ -ray spectrum can be seen in Fig. 5a. From that, a value for the transition energy of  $44.1(2) \text{ keV}$  was obtained in comparison to the value of  $43.7(2) \text{ keV}$  of Ref. [19]. The time distribution belonging to that transition is shown in the inset of Fig. 5a. Figure 5b confirms the assignment by showing the projection of a  $\gamma$ - $\gamma$ -matrix gated on 44 keV. The labelled transitions (470, 667, 1248 and 1505 keV) belong to the decay cascade following the isomeric  $(15^+)$  state.

The time spectrum in the inset of Fig. 5a was obtained using an acquisition range from 600 ns to  $20 \mu\text{s}$  in order to properly display a range of several isomer half-lives. Despite the low statistics, the obtained half-life is consistent with the literature, showing that this transition belongs to the  $(15^+)$  isomer. Due to higher statistics, for determining the half-life another time spectrum was generated by setting an energy gate on the  $667 \text{ keV } (13^+) \rightarrow (11^+)$  transition following the decay of the  $(15^+)$  isomer. The decay curve can be seen in one of the panels of Fig. 2, yielding a half-life of  $T_{1/2} = 1.55(2) \mu\text{s}$ . This result is consistent with the literature value of  $1.56(2) \mu\text{s}$  [42] for the  $(15^+)$  isomer at  $2680 \text{ keV}$  in  $^{96}\text{Ag}$ .

### C. Isomeric Ratios and the Sharp Cut-Off Model

The population of an isomeric state in a nuclear reaction is described by the isomeric ratio summarised in Eq. 1. In this experiment, 25 isomeric ratios have been determined and five of them for the first time. The new ratios belong to isomers in  $^{90}\text{Nb}$  [43–45],  $^{92}\text{Nb}$  [45, 46],  $^{94}\text{Rh}$  [47] and  $^{96}\text{Cd}$  [24]. The experimental values from this work can be found in the third column of Tab. II. For calculating the  $f_2$  and  $f_3$  factors, isomer half-lives from this work were used whenever possible. For  $^{96}\text{Cd}$  ( $12^-, 13^-$ ) the value  $197^{+19}_{-17} \text{ ns}$  [24], for  $^{95}\text{Ag}$  ( $23/2^+$ )  $1.8(2) \text{ ms}$  [48], for  $^{95}\text{Ag}$  ( $33/2$ )  $38(3) \mu\text{s}$  [48] while for the

others literature values from Ref. [42] were used. Table II additionally shows also isomeric ratios from Ref. [19] as well as different theoretical values. First, a comparison to theoretical ratios  $R_{theo}$  will be discussed. Then, the results obtained in this work are compared to the previous study.

The probability that an observed population of an isomeric state originates from the initial population of states in the reaction can be estimated using the sharp cut-off model (SCM) of fragmentation reaction. This model was first introduced by de Jong, Ignatyuk and Schmidt [49] and requires the spin distribution of the final fragments. By making use of the statistical abrasion-ablation model [50], the spin distribution  $P_J$  can be expressed as a function of the fragment's spin  $J$ ,

$$P_J = \frac{2J+1}{2\sigma_f^2} e^{-J(J+1)/2\sigma_f^2}, \quad (6)$$

where  $\sigma_f$  is the spin distribution width of the SCM given by:

$$\sigma_f^2 = \langle j_z^2 \rangle \frac{(A_p - A_f)(\nu A_p + A_f)}{(\nu + 1)^2 (A_p - 1)}. \quad (7)$$

In Eq. 7,  $\langle j_z^2 \rangle$  is the average square of the spin projection and is calculated via

$$\langle j_z^2 \rangle = \kappa A_p^{2/3} \left( 1 - \frac{2}{3}\beta \right), \quad (8)$$

where  $\kappa$  is a constant depending the angular momentum distribution of the potential (0.16 for Woods-Saxon) and  $\beta$  the quadrupole deformation parameter. In the region around the doubly-magic, spherical  $^{100}\text{Sn}$  this deformation is negligible and set to zero.  $A_p = 124$  is the projectile mass number ( $^{124}\text{Xe}$ ) and  $A_f$  the mass of the final fragment. The parameter  $\nu$  describes the mean number of ablated nucleons per abrasion of one nucleon. Depending on the primary beam energy, different values between  $\nu = 2$  and  $\nu = 0.5$  have been used in previous studies [19, 30, 31, 33, 51].

According to the SCM, the theoretical isomeric ratio  $R_{theo}$  can be obtained by integrating the spin distribution probability as defined in Eq. 6 from the isomeric spin  $J_m$  up to infinity

$$R_{theo} = \int_{J_m}^{\infty} P_J dJ = e^{-J_m(J_m+1)/2\sigma_f^2}. \quad (9)$$

Equation 9 is based on the assumption that an isomer with spin  $J_m$  is only populated through spin-decreasing transitions from  $J > J_m$  states. Furthermore,  $R_{theo}$  includes every transition with  $J > J_m$  and, hence, can be interpreted as an upper limit of the isomeric ratio.

Calculations for different  $\nu$  values (0.5, 1.0, 2.0) were performed and can be found in the last three columns of Tab. II. The theoretical values using  $\nu = 0.5$  describe generally well most isomers with  $J_m > J_{gs}$ . The largest deviations are in the order of 50% which is remarkable considering the simplified assumptions of the SCM. The core-excited ( $19^+$ ) isomer in  $^{96}\text{Ag}$  and ( $12^+$ ) isomer in  $^{98}\text{Cd}$  are better described when increasing  $\nu$  to 1.0. This can be explained by the fact that increasing  $\nu$  is equivalent to more evaporated nucleons per abrasion, generating a larger average angular momentum transfer, which is necessary for the high-spin core-excitations. For isomers with a spin smaller than the ground state occurring in odd-odd nuclei, the  $R_{theo}$  overestimates  $R_{exp}$  by orders of magnitude. This is due to the assumption the model is based on. In Eq. 9, the integral includes all transitions with  $J > J_m$ . If  $J_m < J_{gs}$ , it would correspond to isomer population by decay paths via the ground state, which is clearly not the case.

In order to properly estimate the isomeric ratio if the ground state has a higher spin than the isomer, we change the limits of integration in Eq. 9 to be taken from zero up to the isomeric spin. Changing the limits results in a modified expression for  $R_{theo}$  given by

$$R'_{theo} = \int_0^{J_m} P_J dJ = 1 - e^{-J_m(J_m+1)/2\sigma_f^2} = 1 - R_{theo}. \quad (10)$$

The result from Eq. 10 describes the population arising only from spin-increasing transitions. This interpretation is considered for the first time here and the values calculated by Eq. 10 are present in Tab. II in addition to the results obtained from Eq. 9. The agreement with unity of the ratio  $R_{exp}/R_{theo}$  is significantly improved as can be seen in the graphical comparison shown in Fig. 6. Considering the proper ratio  $R_{exp}/R_{theo}$  or  $R_{exp}/R'_{theo}$  in Tab. II, the experimental values are reproduced in most of the cases and the maximum deviation is a factor of four. Note the significant improvement on the description of the values with  $J_m < J_{gs}$  compared to Refs. [19, 41]. In addition, it is important to note that  $R_{exp}/R_{theo}$  values further away from the line of unity are mostly smaller than one. This means that  $R_{theo} \geq R_{exp}$ , corresponding to the fact that the SCM provides an upper limit of the experimental isomeric ratios. Furthermore,  $\nu$  should be even smaller than 0.5 for very low spins, see  $J_m = 2$  states in Tab. II.

The results on isomeric ratios in the vicinity of  $^{100}\text{Sn}$  previously obtained in a similar experiment at the RIBF [19] are listed in the fourth column of Tab. II. The reaction was the same but slightly different separator settings were used.

Table II. Isomeric ratios determined in this work compared to theoretical calculations and results by Park et al. [19]. The calculations were carried out using the SCM and Eq. 9. New isomeric ratios are highlighted in boldface and results that differ by more than  $3\sigma$  from Ref. [19] are marked with an asterisk. The values in curly brackets are calculated with Eq. 10

Nucleus	$J^\pi$	$R_{exp}$ [%]		$R_{theo}$ $\{R'_{theo}\}$ [%]		
		This work	Ref. [19]	$\nu = 0.5$	$\nu = 1.0$	$\nu = 2.0$
$^{88}\text{Zr}$	$8^+$	46(9)	69(5)	62.9	55.8	43.7
$^{90}\text{Nb}$	$(11^-)$	15(4)	16(3)	41.1	32.6	20.2
	$6^+ \text{ }^a$	<b>6.6(1.4)</b>	-	75.4	70.0	60.1
				{24.6}	{30.0}	{39.9}
$^{91}\text{Nb}$	$(17/2^-) \text{ }^a$	33(11)	47(12)	57.3	49.5	36.6
$^{92}\text{Nb}$	$(2)^- \text{ }^a$	<b>2.2(1.3)</b>	-	95.9	94.8	92.6
	$(11^-) \text{ }^a$	<b>42(7)</b>	-	39.4	30.7	18.5
$^{90}\text{Mo}$	$8^+$	60(20)	61(3)	61.6	54.2	41.8
$^{92}\text{Mo}$	$8^+$	28(14)	48(10)	60.2	52.5	39.8
$^{92}\text{Tc}$	$(4^+)$	21(10)	10(1)	86.8	83.6	77.4
				{13.2}	{16.4}	{22.6}
$^{93}\text{Tc}$	$(17/2^-)$	70(30)	54(5)	55.7	47.6	34.6
$^{92}\text{Ru}$	$(8^+)$	36(4)	<65	60.2	52.5	39.8
$^{93}\text{Ru}$	$(21/2)^+$	39(5)	53(2)	41.7	33.0	20.4
$^{94}\text{Ru}$	$8^+$	53(6)	68(6)	58.6	50.6	37.7
$^{92}\text{Rh}$	$(4^+)$	8.3(1.2)	7(3)	86.8	83.6	77.4
				{13.2}	{16.4}	{22.6}
$^{94}\text{Rh}$	$(2^+) \text{ }^a$	<b>1.1(4)</b>	-	95.6	94.5	92.2
				{4.4}	{5.6}	{7.8}
$^{94}\text{Pd}$	$(19^-)$	7(3)	7(3)	5.9	2.8	0.6
	$(14^+)$	15(2)*	30(1)	21.0	13.7	5.8
$^{96}\text{Pd}$	$(8^+)$	51(6)*	76(1)	56.8	48.5	35.3
$^{95}\text{Ag}$	$(33/2) \text{ }^b$	5.9(7)	7.7(7)	11.0	6.0	1.7
	$(23/2^+) \text{ }^b$	40(6)	41(7)	33.4	24.7	13.4
$^{96}\text{Ag}$	$(19^+)$	2.2(1.6)	1.4(8)	5.0	2.2	0.4
	$(15^+)$	12(2)	18.7(4)	15.2	9.0	0.6
	$(13^-)$	11(1)	12(1)	23.9	16.1	7.2
$^{98}\text{Ag}$	$(4^+)$	18(4)	4(1)	84.6	83.6	77.4
				{15.4}	{16.4}	{22.6}
$^{96}\text{Cd}$	$(12^-) \text{ }^c$	<b>12(4)</b>	-	29.3	20.9	10.5
$^{96}\text{Cd}$	$(13^-) \text{ }^c$	<b>12(4)</b>	-	23.9	16.1	7.2
$^{98}\text{Cd}$	$(12^+)$	18(4)	10(1)	27.1	18.8	9.0
	$(8^+) \text{ }^a$	58(7)	97(36)	54.8	46.2	32.8

<sup>a</sup>  $T_{1/2}$  of the isomer taken from Literature [42].

<sup>b</sup> For a discussion of  $J^\pi$  and  $T_{1/2}$  of isomers in  $^{95}\text{Ag}$  see Ref. [48].

<sup>c</sup> Alternative assignment. For a discussion of  $J^\pi$  and  $T_{1/2}$  of the isomer in  $^{96}\text{Cd}$  see Ref. [24].

The experimental setup differed only by the active stopper WAS3ABI [52]. The only difference in the determination of isomeric ratios was the lack of a prompt flash correction factor,  $f_1$ , defined in Eq. 2 which was included in this work and ranged from 90 to 98%. Overall, the results for the experimental isomeric ratios are in a good agreement with Ref. [19] taking

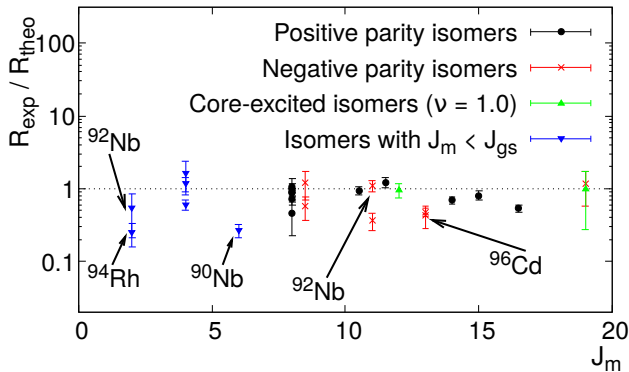


Figure 6. (Colour online) Isomeric ratios: comparison between experimental and theoretical values expressed as the ratio  $R_{exp}/R_{theo}$ . If not denoted otherwise, the theoretical isomeric ratios were calculated using  $\nu = 0.5$ . For isomers with  $J_m < J_{gs}$  the theoretical value was obtained using Eq. 10. Figure adapted from Ref. [41] and new experimental values are labelled with the respective isotope. In the case of  $^{96}\text{Cd}$  only one of the ratios, i.e. for the alternative assignment ( $13^-$ ) has been plotted. For details see text and Tab. II.

the error bars into account. Note that all experimental values obtained in this work are closer to theoretical values using  $\nu = 0.5$  and Eq. 9 or Eq. 10 than the values of Ref. [19], which may support the usefulness of the  $f_1$  correction. However, there are a few cases that deviate by more than  $3\sigma$  (labelled by asterisks in Tab. II), for which the main reasons for the discrepancies of  $R_{exp}$  between this work and Ref. [19] are most probably the different separator settings corresponding to different momentum cuts, which have a strong influence on the population of isomeric states, see, for example, Ref. [53].

#### IV. CONCLUSIONS

In summary,  $\gamma$ -decaying isomers in the  $^{100}\text{Sn}$  region produced at the RIBF of the RIKEN Nishina Center and separated in the two-stage fragment separator BigRIPS were investigated

with the EURICA setup. Half-life and transition energy measurements were performed. The obtained results are consistent with literature values and improve the relative uncertainty in some cases. The second observation of recently discovered low-energy isomeric transitions in  $^{92}\text{Rh}$  and  $^{96}\text{Ag}$  confirms their existence and the transition energy decaying from the isomer in  $^{92}\text{Rh}$  is given with higher precision. The half-life of the recently proposed ( $4^+$ ) isomer in  $^{92}\text{Rh}$  was remeasured reducing its uncertainty by a factor of four. The reduced transition strengths are largely consistent with SM calculations in the PG model space employing the empirical SLGTOPN interaction. Furthermore, isomeric ratios around  $N = Z = 50$  were remeasured including five new results for isomers in  $^{90}\text{Nb}$ ,  $^{92}\text{Nb}$ ,  $^{94}\text{Rh}$  and  $^{96}\text{Cd}$ . The values exhibit an overall agreement with the previous study [19] and differences are explained by use of dissimilar experimental settings or accounting for a prompt flash correction factor,  $f_1$ , in the present work. An extensive analysis based on the SCM was performed in order to describe these new findings. Most of the  $R_{exp}$  can be reproduced by this model. For  $J_m < J_{gs}$ , a modified population integral was used for the first time. Independently of other experiments, no experimental evidence for the predicted core-excited isomer in  $^{100}\text{Sn}$  was found and further effort has to be made towards the design of future experiments to study excited states in  $^{100}\text{Sn}$ .

#### ACKNOWLEDGMENTS

This work was carried out at the RIBF operated by the RIKEN Nishina Center, RIKEN and CNS, University of Tokyo. We acknowledge the EUROBALL Owners Committee for the loan of germanium detectors and the PreSpec Collaboration for the readout electronics of cluster detectors. This work was partly supported by the German BMBF under Contract No. 05P12PKFNE and No. 05P15PKFNA, the U.S. Department of Energy under grant No. DE-FG02-91ER40609, JSPS KAKENHI grant No. KAKENHI 25247045 and the UK STFC under grants ST/J000124/1, ST/L005727/1 and ST/P003885/1. GH was supported by the Bonn-Cologne Graduate School of Physics and Astronomy.

- 
- [1] R. K. Wallace and S. E. Woosley, *Astrophys. J. Suppl.* **45**, 389 (1981).  
 [2] H. Schatz *et al.*, *Phys. Rev. Lett.* **86**, 3471 (2001).  
 [3] T. Faestermann, M. Górska, and H. Grawe, *Prog. Part. Nucl. Phys.* **69**, 85 (2013).  
 [4] C. B. Hinke *et al.*, *Nature* **486**, 341 (2012).  
 [5] B. Cederwall *et al.*, *Nature* **469**, 68 (2011).  
 [6] O. Häusser *et al.*, *Nucl. Phys. A* **293**, 248 (1977).  
 [7] E. Nolte and H. Hick, *Z. Phys. A* **305**, 289 (1997).  
 [8] H. Grawe and H. Haas, *Phys. Lett. B* **120**, 63 (1983).  
 [9] D. Alber *et al.*, *Z. Phys. A* **332**, 129 (1989).  
 [10] M. Palacz *et al.*, *Phys. Rev. C* **86**, 014318 (2012).  
 [11] M. Lipoglavšek *et al.*, *Phys. Rev. C* **72**, 061304 (2005).  
 [12] M. Lipoglavšek *et al.*, *Phys. Rev. C* **66**, 011302(R) (2002).  
 [13] P. Boutachkov *et al.*, *Phys. Rev. C* **84**, 044311 (2011).  
 [14] A. Blazhev *et al.*, *Phys. Rev. C* **69**, 064304 (2004).  
 [15] A. Blazhev *et al.*, *J. Phys. Conf. Series* **205**, 012035 (2010).  
 [16] F. J. D. Serduke, R. D. Lawson, and D. H. Gloeckner, *Nucl. Phys. A* **256**, 45 (1976).  
 [17] R. Gross and A. Frenkel, *Nucl. Phys. A* **267**, 85 (1976).  
 [18] F. Nowacki, *Nucl. Phys. A* **704**, 223 (2002).  
 [19] J. Park *et al.*, *Phys. Rev. C* **96**, 044311 (2017).  
 [20] P. A. Söderström *et al.*, *Nucl. Instr. Meth. Phys. Res. B* **317**, 649 (2013).  
 [21] K. Moschner *et al.*, *EPJ Web of Conf.* **93**, 01024 (2015).  
 [22] K. Moschner, Ph.D. thesis, Universität zu Köln (2016).  
 [23] P. J. Davies *et al.*, *Phys. Lett. B* **767**, 474 (2017).  
 [24] P. J. Davies *et al.*, *Phys. Rev. C* **99**, 021302 (2019).  
 [25] N. Fukuda *et al.*, *Nucl. Instr. Meth. Phys. Res. B* **317**, 323 (2013).  
 [26] T. Kubo *et al.*, *Prog. Theor. Exp. Phys.* **2012**, 03C003 (2012).  
 [27] N. Warr, A. Blazhev, and K. Moschner, *EPJ Web of Conf.* **93**, 07008 (2015).

- [28] O. B. Tarasov and D. Bazin, *Nucl. Instr. Meth. Phys. Res. B* **266**, 4657 (2008).
- [29] T. Kibédi *et al.*, *Nucl. Instr. Meth. Phys. Res. A* **589**, 202 (2008).
- [30] M. Pfützner *et al.*, *Phys. Rev. C* **65**, 064604 (2002).
- [31] M. Bowry, Ph.D. thesis, University of Surrey (2013).
- [32] M. Bowry *et al.*, *Phys. Rev. C* **88**, 024611 (2013).
- [33] K. A. Gladnishki *et al.*, *Phys. Rev. C* **69**, 024617 (2004).
- [34] B. A. Brown and W. D. M. Rae, *Nucl. Data Sheets* **120**, 115 (2014).
- [35] H. Herndl and B. A. Brown, *Nucl. Phys. A* **627**, 35 (1997).
- [36] D. Rudolph *et al.*, *Nucl. Phys. A* **587**, 181 (1995).
- [37] O. Kavatsyuk *et al.*, *Eur. Phys. J. A* **31**, 223 (2002).
- [38] B. A. Brown, D. B. Fossan, P. M. S. Lesser, and A. R. Poletti, *Phys. Rev. C* **13**, 1194 (1976).
- [39] T. S. Brock *et al.*, *Phys. Rev. C* **82**, 061309(R) (2010).
- [40] A. Amusa and R. D. Lawson, *Z. Phys. A* **307**, 333 (1982).
- [41] G. Haefner *et al.*, *Acta Phys. Pol. B* **50**, 431 (2019).
- [42] G. Audi *et al.*, *Chin. Phys. C* **41**, 030001 (2017).
- [43] E. A. Ivanov, *Rev. Roumaine Phys.* **12**, 885 (1967).
- [44] R. E. Holland, R. D. Lawson, and F. J. Lynch, *Ann. of Phys.* **63**, 607 (1971).
- [45] H. Bartsch, K. Huber, U. Kneissl, and H. Krieger, *Z. Phys.* **A285**, 273 (1978).
- [46] R. B. Duffield and S. H. Vegors Jr., *Phys. Rev.* **112** (1958).
- [47] L. Batist *et al.*, Tech. Rep. GSI 2004-1 (2004).
- [48] A. Blazhev *et al.*, in preparation.
- [49] M. de Jong, A. V. Ignatyuk, and K.-H. Schmidt, *Nucl. Phys. A* **613**, 435 (1997).
- [50] J.-J. Gaimard and K.-H. Schmidt, *Nucl. Phys. A* **531**, 709 (1991).
- [51] J. M. Daugas *et al.*, *Phys. Rev. C* **63**, 064609 (2001).
- [52] S. Nishimura *et al.*, *Prog. Theor. Exp. Phys.* **2012**, 03C006 (2012).
- [53] E. C. Simpson, J. A. Tostevin, Zs. Podolyák, P. H. Regan, and S. J. Steer, *Phys. Rev. C* **82**, 037602 (2012).